Temporal reflection as a spectral-broadening mechanism in dual-pumped dispersion-decreasing fibers and its connection to dispersive waves

Aku Antikainen, Francisco R. Arteaga-Sierra, and Govind P. Agrawal

Phys. Rev. A **95**, 033813 — Published 16 March 2017

DOI: 10.1103/PhysRevA.95.033813

Temporal Reflection as a Spectral Broadening Mechanism in Dual-Pumped Dispersion-Decreasing Fibers and its Connection to Dispersive Waves

Aku Antikainen,* Francisco R. Arteaga Sierra, and Govind P. Agrawal†
The Institute of Optics, University of Rochester, Rochester NY 14627
(Dated: February 3, 2017)

We show that temporal reflections off a moving refractive index barrier play a major role in the spectral broadening of a dual-wavelength input inside a highly nonlinear, dispersion decreasing fiber. We also find that a recently developed linear theory of temporal reflections works well in predicting the reflected frequencies. Successive temporal reflections from multiple closely spaced solitons create a blue-shifted spectral band, while continuous narrowing of solitons inside the dispersion decreasing fiber enhances Raman-induced red shifts, leading to supercontinuum generation at relatively low pump powers. We also show how dispersive wave emission can be considered a special case of the more general process of temporal reflections. Hence our findings have implications on all systems able to support solitons.

INTRODUCTION

The mathematical equations governing light propagation in optical fibers have established connections between nonlinear fiber optics and seemingly unrelated fields such as Bose-Einstein condensates [1], plasma physics [2], and water waves [3]. Fiber optics offers a convenient laboratory-scale platform for studying systems covered by the nonlinear Schrödinger equation. One of the extreme nonlinear phenomena occurring in optical fibers is supercontinuum (SC) generation [4], which is of great interest to the broader physics and engineering community because of its applications in optical coherence tomography [5], high-precision metrology [6], communication systems [7], and optical pulse-shaping [8].

SC generation in photonic crystal fibers (PCFs) has been studied extensively over the past decade [4, 9]. The dispersion of a PCF can be made to change along its length either during the manufacturing process or by tapering it afterwards. SC generation has been studied in both kinds of dispersion-varying fibers [10]. Typically the fiber is pumped in the anomalous-dispersion regime, and the magnitude of the dispersion parameter β_2, defined as $\beta_2 = d^2\beta/d\omega^2$ where $\beta(\omega)$ is the modal propagation constant at frequency ω, is made to decrease along fiber's length. Such fibers are referred to as dispersion-decreasing fibers (DDFs). The beneficial effect of decreasing $|\beta_2|$ on the spectral width of an optical pulse is evident in the context of solitons, as decreasing $|\beta_2|$ causes them to compress temporally, which broadens their spectrum and also causes them to red-shift faster through the Raman effect [11, 12]. In practice, tapering a fiber will also decrease its core size leading to broader SC spectra simply due to enhanced nonlinearities [10, 13].

When the input to a nonlinear fiber is a continuous wave (CW) or a long pulse at a wavelength in the anomalous-dispersion regime of the fiber, spontaneous modulation instability (MI) breaks it into a train of much shorter pulses [12]. Spontaneous noise-seeded MI leads to incoherent supercontinua [14]. However, MI can also be induced by modulating the input at an appropriate frequency, resulting in better coherence properties [15]. In this case, MI causes the modulation sidebands to grow, and the cascaded effect can yield frequency combs. Another way to induce MI is to pump the fiber with two (or more) pumps of different wavelengths. SC and frequency comb generation using dual-wavelength pumping has been explored in numerous studies [16–21]. The dual-pump configuration can have significant advantages over single-CW pumping. Demircan et al. [22] considered two pulses on opposite sides of the zero-dispersion wavelength (ZDW). The solitonic input pulse created a moving temporal refractive-index barrier for the other pulse propagating in the normal dispersion regime. The other pulse then scattered off this barrier and created new spectral components in a quasi-continuous manner, leading to a very broad and relatively flat SC spectrum.

Using the dual-pumping case as an example, in this Letter we reveal the origin of the blue components during SC generation in DDFs. This explains previous experimental results on enhanced blue side spectral broadening [10] as well as our recent observations about longitudinally varying dispersion being beneficial for dual-pump SC generation but detrimental for a single CW pump [23]. The origin of the blue components then brings us to an important result: a connection between dispersive wave (DW) emission and the more general phenomenon of temporal reflection [24]. Dual pumping creates an amplitude-modulated input signal, which evolves nonlinearly into a train of fundamental solitons that are then compressed temporally by decreasing $|\beta_2|$. While adiabatic soliton compression due to varying dispersion extends the spectrum to the red side, here we show that the blue side of the spectrum is also significantly affected through multiple reflections of the pump remnants at the soliton-induced index barriers. In previous work, scattering of DW's off solitons led to spectral broadening only under carefully crafted input conditions [22, 25]. In contrast, our approach allows temporal reflection to occur spontaneously, with little sensitivity to the input condi-

tions. Furthermore, the periodic nature of the emerging soliton train effectively creates temporal waveguides for the blue frequency components, and the waves can keep reflecting and remain partially trapped between two adjacent solitons. This wave-trapping phenomenon continues to be a topic of contemporary research [26].

NUMERICAL MODEL

We use the generalized nonlinear Schrödinger equation that has been shown to accurately model nonlinear propagation down to the few-cycle regime [9]. This equation can be written as [12]

$$\frac{\partial A}{\partial z} + \frac{\alpha}{2}A - \sum_{n\geqslant 2}\frac{i^{n+1}}{n!}\beta_n\frac{\partial^n A}{\partial T^n} = i\gamma\left(1 + i\tau_s\frac{\partial}{\partial T}\right)\left(A(z,T)\int_{-\infty}^{\infty}R(T')\left|A(z,T-T')\right|^2 dT'\right), \quad (1)$$

where A is the complex amplitude of the electric field, $T = t - z/v_g$ is the retarded time in a frame moving with the group velocity v_g at a chosen central frequency ω_0, α accounts for fiber losses, and γ is the nonlinear parameter. Further, the sum is over dispersive terms with the parameters β_n, defined as $\beta_n = (d^n\beta/d\omega^n)$ and evaluated at ω_0. For a DDF, in general, all dispersion parameters β_n are functions of z. In this work, however, only β_2 changes linearly with z, and the higher-order terms as well as the nonlinearity are kept constant. Equation (1) is solved numerically using the split-step Fourier method [12].

The input consists of two CW's of equal power and different frequencies centered around $\nu_0 = \omega_0/(2\pi) = c_0/\lambda_0$, where c_0 is the vacuum speed of light and $\lambda_0 = 1.06\ \mu$m. Quantum shot-noise is also included by adding one photon with random phase per mode [9]. The frequency separation $\Delta\nu$ between the two pumps is varied from 25 GHz to 1 THz. The nonlinear parameter is $\gamma = 91.6\ (\mathrm{W\,km})^{-1}$ at the center frequency ω_0. β_2 at ω_0 increases linearly from -8.56 to 5 $\mathrm{ps}^2/\mathrm{km}$ over the 150 m length of the fiber. The dispersion curve at the fiber's input end is shown in Fig. 1.

The nonlinear response function, $R(t) = 0.82\delta(t) + 0.18h_{\mathrm{R}}(t)$, includes both the delayed Raman response h_{R} and the instantaneous [12] Kerr-type electronic response. The convolution integral on the right-hand side of Eq. (1) is done in the frequency domain where the Raman contribution is modeled through the full experimental Raman spectrum of silica [27]. Self-steepening is governed by the shock time scale $\tau_s = 0.563$ fs. The fiber lengths considered were 150 meters or less, and since losses for PCF's of such lengths can be less than 0.15 dB [28], they were ignored for simplicity by setting $\alpha = 0$.

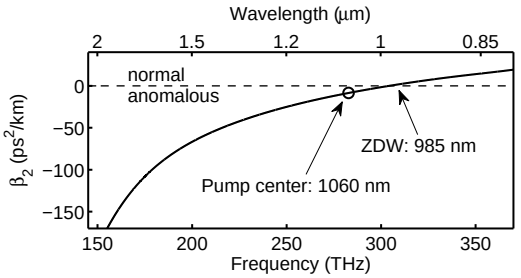

FIG. 1. Dispersion parameter β_2 at the input end of the fiber. The circle denotes ν_0. The zero-dispersion wavelength of the PCF is 985 nm.

ROLE OF TEMPORAL REFLECTIONS

Figure 2 shows the temporal and spectral evolution of a dual-pump input inside a DDF (frequency separation $\Delta\nu = 400$ GHz). The total input power of 1 W corresponds to a peak power of only 2 W at the location of each temporal peak. The input acts as a train of cosine-shaped pulses with a full width at half-maximum of 1.25 ps. During the first 20 meters, the pulses compress temporally as they undergo self-phase modulation (SPM). The central peak of each individual pulse then starts adjusting to become a fundamental soliton. During these stages the spectrum is still comb-like.

Once solitons are formed, the soliton self-frequency shift (SSFS) starts red-shifting them. Moreover, the red-shift is accelerated compared to a fiber with constant dispersion due to a decrease in $|\beta_2|$ along the fiber length. This is because of soliton compression making the solitons more intense and shorter in time. The rate of SSFS scales inversely with the fourth power of soliton duration [12] and thus the red-shift becomes greatly enhanced. Since the input power is too low for modulation instability to amplify the shot noise to observable levels, the first stages of signal evolution are governed solely by the SPM phenomenon.

Until each soliton has decelerated enough to temporally overlap with the remnants of the neighboring pulse, each pulse follows single-pulse evolution dynamics. After 65 meters of propagation, the pump remnants of the adjacent pulse see a moving refractive-index barrier caused by solitons, resulting in temporal reflections that create new frequency components between 970 and 980 nm [24]. Most of the pump remnants pass through this index barrier and undergo further temporal reflections creating new spectral components first between 990 nm and 1.02 μm, then 1.02 μm and 1.025 μm, and finally between 1.03 μm and 1.04 μm (after 130 m of propagation).

In a recent study by Plansinis et al. [24] temporal reflections, occurring because of an abrupt temporal change in the refractive index, were studied and the spectral shift of the reflected light was predicted analytically using the

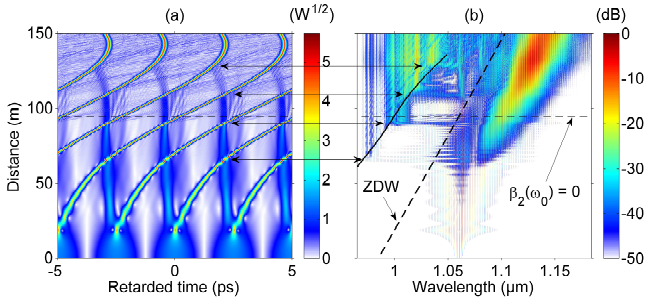

FIG. 2. Temporal (a) and spectral (b) evolutions of a dual-pump input inside a DDF. (a) shows the square root of the intensity on a linear scale in $\sqrt{\text{W}}$, and (b) shows the normalized spectral intensity in decibels. The two pumps are separated in frequency by 400 GHz and their total power is 1 W. The dashed black line shows the distance at which $\beta_2 = 0$ at the pumps' center wavelength. Double arrows mark locations of temporal reflections in (a) together with the corresponding wavelengths in (b). The solid black line in (b) shows the theoretical prediction of the temporal reflection model discussed in the text. The dashed line shows the zero-dispersion wavelength.

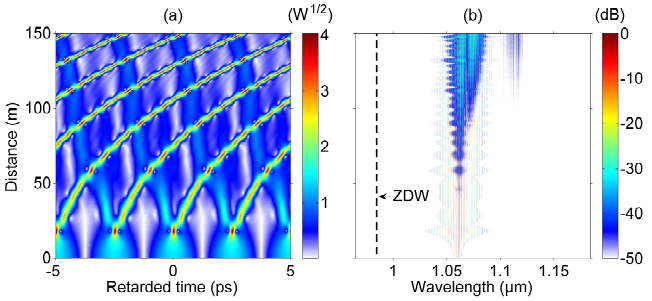

FIG. 3. Temporal (a) and spectral (b) evolutions of a dual-pump input under conditions identical to those in Fig. 2 except that the dispersion is kept constant along the PCF length.

conservation of photon momentum during the reflection process. In their theory, the frequency ω of reflected light is obtained from

$$\Delta\beta_1(\omega - \omega_0) + \sum_{n\geq 2} \frac{\beta^n}{n!}(\omega - \omega_0)^n = 0, \qquad (2)$$

where the Taylor expansion has been done around the incident frequency ω_0 and $\Delta\beta_1 = \beta_1(\omega_0) - 1/V_B$, V_B being the velocity of the moving refractive index barrier. The trivial solution $\omega = \omega_0$ corresponds to the incident wave, and the other solution, if it exists, provides the frequency of the reflected wave.

In the case studied in this Letter, the intense narrow solitons act as the moving refractive-index barriers. Therefore, the barrier velocity V_B is the inverse of the first-order dispersion coefficient $\beta_1(\omega_s)$, where ω_s is the soliton's center frequency. By virtue of the retarded time coordinate used, $\beta_1(\omega_0) = 0$, and the difference $\Delta\beta_1$ in Eq. (2) reduces to $\Delta\beta_1 = -\beta_1(\omega_s)$. To determine the value of $\beta_1(\omega_s)$, we traced the curved trajectory of a soliton in Fig. 2(a) and fitted a polynomial spline to it, expressing the location T_p of the soliton peak as a function of z. The derivative dT_p/dz then yields $\beta_1(\omega_s)$. Knowing $\beta_1(\omega_s)$, we calculated ω_s and checked that it agreed with the spectral peak of the solitons. The calculated $\beta_1(\omega_s)$ was then used to determine the wavelength of the reflected wave when the pump remnants centered around 1.06 μm reflect off the solitonic index barrier. The solid black line in Fig. 2(b) shows the predictions for the reflected wavelength based on Eq. (2). As seen in this figure, the theoretical predictions agree quite well with the numerical results.

By looking at Fig. 2(b) we note that the input spectrum has broadened considerably at a distance of 65 m (just before the first reflection), forming a frequency comb spanning from 1.02 μm to 1.12 μm through dual-pump enhanced SPM [20]. Since there is a band of (discrete) frequencies that can reflect off the solitonic index barriers, the reflected frequencies also form bands around the theoretically predicted curve (solid black line). The width and position of these bands depend on the width of the incident band, the dispersion, and the central wavelength of the solitons [through $\beta_1(\omega_s)$], as evident from Eq. (2). Furthermore, the theory of Ref. [24] does not account for nonlinearities, which affect the propagation constants of both the incident and reflected waves (owing to the Kerr effect). In addition, the nonlinear effects are expected to be different in magnitude for the incident and reflected waves, as the latter is much weaker than the former one.

To clarify the drastic effects of temporal reflections on the blue side of the output spectra, we also performed simulations in constant dispersion fibers with the same dispersion curve shown in Fig. 1 for all z. Figure 3 shows the temporal and spectral evolutions of the same input signal in this case and should be compared with Fig. 2 where dispersion varies along the fiber length. It is remarkable how narrow the output spectrum is in Fig. 3(b) when compared to that in Fig. 2(b). The additional spectral broadening in Fig. 2(b) has two sources: On the red side, it is due to soliton compression and enhanced SSFS of the narrower solitons. In contrast, on the blue side, spectral broadening is due to the formation of blue-shifted spectral bands resulting from temporal reflections. Note that there is no visible DW emission in either case, and all the blue-shifted components that are present in Fig. 2(b) but not in Fig. 3(b) are solely due to temporal reflections of the pump remnants off the solitons.

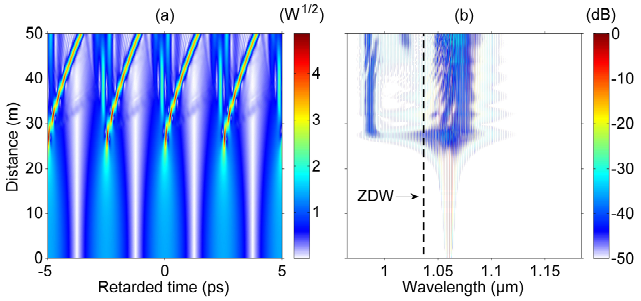

FIG. 4. Temporal (a) and spectral (b) evolutions under conditions identical to those in Fig. 3 except that the value of β_2 at the pump-center wavelength was changed to -2.684 ps^2/km.

DISPERSIVE WAVES AND TEMPORAL REFLECTIONS

The absence of a DW in Fig. 3 is, at first, somewhat puzzling since such waves are often generated when solitons form. On further investigation, we find that the reason behind the lack of temporal reflections in Fig. 3(b) is related to the shape of the dispersion curve, which causes Eq. (2) to have only one solution $\omega = \omega_0$ such that no solution exists for a reflected wave. Since no temporal reflections can occur, all pump remnants incident on a solitonic index barrier simply pass through it (temporal refraction), without a significant change in their frequencies [24]. We stress that this behavior is due to the presence of dispersion terms beyond the third order in our simulations.

To clarify this issue further, we carried out additional numerical simulations. Figure 4 shows the temporal and spectral evolutions under conditions identical to those in Fig. 3, except that the value of β_2 at the pump's center wavelength was -2.684 ps^2/km rather than -8.56 ps^2/km like in Fig. 3. This value of β_2 corresponds to its value in Fig. 2 at a distance of 65 m, which is the location of the first temporal reflection. As in Fig. 3, the input beating signal reshapes to form a periodic train of solitons, but unlike in Fig. 3, now each soliton emits a DW soon after its formation at a distance of 30 m.

The wavelength of a DW can be calculated from the phase-matching condition [12]:

$$\sum_{n\geq 2} \frac{\beta^n}{n!}(\omega-\omega_0)^n - (\omega-\omega_0)/v_g - \gamma P_0 = 0, \qquad (3)$$

where P_0 is the soliton's peak power and v_g its group velocity. In practice, the nonlinear term is often small compared to the others and can be neglected to yield the linear phase-matching condition. When $\gamma P_0 = 0$, equation (3) is exactly identical to the temporal reflection equation (2) when $V_B = v_g$ because $\Delta\beta_1 = -1/v_g$ in that situation. When the moving refractive-index boundary is caused by solitons of group velocity v_g, the condition $V_B = v_g$ is automatically satisfied, and Eq. (2) becomes Eq. (3) with $\gamma P_0 = 0$. This indicates that DW emission is a special case of a temporal reflection process. Thus, DW emission in Fig. 4 and the formation of blue-shifted components in Fig. 2 through a temporal reflection are the same phenomenon. The difference can be understood as follows. In Fig. 2 the pump remnants meet and interact with the solitons after they have left the original pulse and slowed down considerably through the SSFS. In contrast, in Fig. 4 the pump remnants on the trailing side of each soliton reflect off that soliton itself as it slows down. In other words, DW generation is a kind of "temporal self-reflection," where the temporal refractive-index boundary is caused by the formation of a soliton in a pulse's central region, and the trailing parts of the same input pulse reflect off this soliton, changing their frequency as required by the process of temporal reflection. Small differences in the wavelengths of the blue components in Figures 2(b) and 4(b) can be attributed to slight differences in the soliton group velocities and peak powers in the two cases.

Interpreting DW emission as a special case of temporal reflection also explains the lack of DW's in Fig. 3. As mentioned earlier, the shape of the dispersion curve in the case of Fig. 3 is such that Eq. (2) admits only one solution ($\omega = \omega_0$), and hence no temporal reflections can occur. As the same equation in the form of Eq. (3) governs DW emission, no such waves are generated either. All pump remnants initially present during soliton formation at a distance of 20 m simply pass through the solitons without reflecting off them.

CONCLUSIONS

Using numerical simulations, we showed how temporal reflections are a key spectral broadening process when two or more closely spaced pulses are transmitted through an optical fiber. To be specific, we focused on a periodically modulated input signal created by launching two CW laser beams at slightly different wavelengths. We compared the output spectra for PCFs with both constant dispersion and longitudinally varying dispersion (a DDF). We found that spectral broadening was enhanced considerably in the case of a DDF and attributed the broadening on the blue side to temporal reflections from a moving refractive-index boundary created by the solitons. We used the recently developed theory of Ref. [24] to predict the reflected frequency bands and found it in agreement with our numerical simulations. Importantly, we interpret DW generation as a special case of temporal reflection, in which the spectral components that reflect off the temporal index boundary have the same or nearly the same frequency as the soliton that produces the temporal boundary, hence connecting temporal reflections to a wider range of physical systems.

* aku.antikainen@rochester.edu
† Also at Laboratory for Laser Energetics, 250 East River Rd, Rochester, NY 14623, USA

[1] Y. V. Bludov, V. V. Konotop, and N. Akhmediev, Phys. Rev. A **80**, 033610 (2009)
[2] J. Williams, Nature Physics **12**, pp. 529–530 (2016)
[3] A. Chabchoub, N. P. Hoffmann, and N. Akhmediev, Phys. Rev. Lett. **106**, 204502 (2011)
[4] J. K. Ranka, R. S. Windeler, and A. J. Stentz, Opt. Lett. **25**(1), pp. 25–27 (2000)
[5] A. F. Fercher, W. Drexler, C. K. Hitzenberger, and T. Lasser, Reports on Progress in Physics **66**(2), 239 (2003)
[6] J. T Woodward, A. W. Smith, C. A. Jenkins, C. Lin, S. W. Brown, and K. R. Lykke, Metrologia **46**(4), S277 (2009)
[7] R. R. Alfano, *The Supercontinuum Laser Source*, (Springer 2016), Chap. 10
[8] B. Schenkel, R. Paschotta, and U. Keller, J. Opt. Soc. Am. B **22**(3), pp. 687–693 (2005)
[9] J. M. Dudley, G. Genty, and S. Coen, Rev. Mod. Phys. **78**, pp. 1135–1184 (2006)
[10] A. Kudlinski, A. K. George, J. C. Knight, J. C. Travers, A. B. Rulkov, S. V. Popov, and J. R. Taylor, Opt. Lett. **14**(12), pp. 5715–5722 (2006)
[11] F. M. Mitschke and L. F. Mollenauer, Optics Letters **11**(10), pp. 659–661 (1986)
[12] G. P. Agrawal, *Nonlinear Fiber Optics*, 5th ed. (Academic Press, 2013)
[13] S. P. Stark, A. Podlipensky, N. Y. Joly, and P. St. J. Russell, J. Opt. Soc. Am. B **27**(3), pp. 592–598 (2010)
[14] D. Solli, C. Ropers, P. Koonath, and B. Jalali, "Optical rogue waves," Nature, **450**, pp. 1054–1057 (2007)
[15] G. Genty and J. M. Dudley, IEEE J. Quantum Electron. **45**(11), pp. 1331–1335 (2009)
[16] T. Schreiber, T. V. Andersen, D. Schimpf, J. Limpert, and A. Tünnermann, Opt. Express **13**(23), pp. 9556–9569 (2005)
[17] E. Räikkönen, G. Genty, O. Kimmelma, M. Kaivola, K. P. Hansen, and S. C. Buchter, Opt. Express **14**(17), pp. 7914–7923
[18] C. Xiong, Z. Chen, and W. J. Wadsworth, J. Lightwave Technol. **27**(11) pp. 1638–1643 (2009)
[19] Y. Wang, C. Xiong, J. Hou, J. Cao, Y. Li, R. Song, and Q. Lu, Applied Optics **50**(17) pp. 2752–2758 (2011)
[20] A. Antikainen and G. P. Agrawal, J. Opt. Soc. Am. B **32**, pp. 1705–1711 (2015)
[21] N. Jia, H. T. Yan, and M. Li, IEEE Photonics Journal, **8**(1), 7100207 (2016)
[22] A. Demircan, S. Amiranashvili, C. Brée, and G. Steinmeyer, Phys. Rev. Lett. **110**, 233901 (2013)
[23] A. Antikainen, F. R. Arteaga Sierra, and Govind P. Agrawal, Frontiers in Optics, FTu1I.6 (2016)
[24] B. W. Plansinis, W. R. Donaldson, G. P. Agrawal, Phys. Rev. Lett. **115**(18), 183901 (2015)
[25] A. Demircan, S. Amiranashvili, C. Brée, U. Morgner, and G. Steinmeyer, Opt. Express **22**(4), pp. 3866–3879 (2014).
[26] Z. Deng, X. Fu, J. Liu, C. Zhao, and S. Wen, Opt. Express **24**(10), pp. 10302–10312 (2016)
[27] R. H. Stolen, J. P. Gordon, W. J. Tomlinson, and H. A. Haus, J. Opt. Soc. Am. B **6**(6), pp. 1159–1166 (1989)
[28] K. Kurokawa, K. Nakajima, K. Tsujikawa, T. Yamamoto, and K. Tajima, J. Lightwave Technol. **27**(11), pp. 1653–1662 (2009)